Scalar Auxiliary Variable Techniques for Nonlinear Transverse String Vibration

Conference Paper · June 2024

CITATIONS
2

READS
44

3 authors:

Riccardo Russo
University of Bologna
16 PUBLICATIONS **13** CITATIONS
SEE PROFILE

Stefan Bilbao
The University of Edinburgh
237 PUBLICATIONS **3,607** CITATIONS
SEE PROFILE

Michele Ducceschi
University of Bologna
75 PUBLICATIONS **448** CITATIONS
SEE PROFILE

Scalar Auxiliary Variable Techniques for Nonlinear Transverse String Vibration

Riccardo Russo [*] **Stefan Bilbao** [**] **Michele Ducceschi** [*]

[*] *Department of Industrial Engineering, University of Bologna, Viale Risorgimento 2, Bologna, Italy*
(e-mail: riccardo.russo19@unibo.it, michele.ducceschi@unibo.it).
[**] *Acoustics & Audio Group, University of Edinburgh, Edinburgh, UK*
(e-mail: sbilbao@ed.ac.uk)

Abstract: The simulation of string vibration is of fundamental importance in musical acoustics. If the vibration amplitude is large then nonlinear phenomena, resulting from large deformations, cannot be neglected, and lead to perceptually salient features. Energy-conserving simulation algorithms found in the literature rely on tailored discretisation choices, making them model–specific. Recently, energy quadratisation–based techniques have been developed, under the assumption that the potential energy is single-signed. These methods allow for the solution of a variety of different nonlinear systems with the same time-stepping procedure, requiring only the evaluation of a specific nonlinear potential. Moreover, they possess an exact numerical energy conservation property, and permit efficient operation. Such methods were previously employed for solving nonlinear string models. In this paper, nonlinear models of transverse string vibration are first semi-discretised in space by means of both finite differences and modal methods. The resulting equations are solved through the use of the Scalar Auxiliary Variable (SAV) technique. Results are then compared against those obtained with model – specific numerical integrators in terms of efficiency and accuracy.

Keywords: Numerical Methods; Hamiltonian Dynamics; Geometric Mechanics

1. INTRODUCTION

The nonlinear vibration of strings is of great perceptual importance, and has seen extensive investigation at the theoretical level. In the earliest simplified models, due to Kirchhoff (1883) and Carrier (1945), longitudinal motion is averaged over the string length, leading to a transverse wave equation with a global amplitude-dependent wave speed. The so-called Kirchhoff-Carrier model was subsequently intensively investigated by Oplinger (1960), Anand (1969), Dickey (1969), Dickey (1980), Gough (1984) and others. More generally, a complete model must include a pointwise coupling between the motion in the two transverse polarisations with longitudinal motion. Such a model is presented by Morse and Ingard (1968), and more general forms have been investigated by Narasimha (1968) and Kurmyshev (2003). Such pointwise nonlinear models, often reduced to one transverse polarization, have been used in various applications in sound synthesis and musical acoustics—see, e.g., Bank and Sujbert (2005) and Chabassier et al. (2013).

Numerical solution techniques have been presented by various authors, especially in the case of the Kirchhoff-Carrier model, where methods based on Volterra series have been applied—see Roze and Hélie (2008). A major consideration for all models of nonlinear string vibration is ensuring numerical stability, particularly as loss is generally quite low in musical strings. To this end, methods based on numerical conservation, and more generally dissipation, of a "pseudo-energy" (henceforth simply "energy") have been used extensively for finite difference schemes for the Kirchhoff-Carrier model (Bilbao and Smith III (2005)) and for more general pointwise nonlinearities in strings (Bilbao (2005), Chabassier et al. (2013)). In the most general case of a geometric string nonlinearity, such schemes are fully implicit, requiring iterative numerical methods such as Newton-Raphson for solution. The computational cost can be prohibitively high. In some cases, when the geometric nonlinearity is simplified to be of cubic type, linearly implicit resolution is possible, avoiding the need for iterative solvers. However, linearly implicit solvers only became available for energy dissipative schemes with the advent of so-called "quadratised" schemes, such as the Invariant Energy Quadratisation (IEQ) approaches. (Yang and Han (2016); Yang et al. (2017)). See Ducceschi and Bilbao (2022) for the present case of nonlinear string vibration. Finally, scalar auxiliary variable (SAV) approaches (Shen et al. (2018)) indicate the possibility of fully explicit and energy-stable resolution, see Bilbao et al. (2023). Further explicit methods for a class of nonlinear ordinary differential equations were given by Lopes et al. (2015).

There is thus a multiplicity of exactly energy-conserving (more generally strictly dissipative) methods available in the case of nonlinear string vibration—all capable of ensuring numerical stability, but with great differences in terms of performance. Part of the focus of this short contribution is to investigate distinctions between different designs of numerical methods. Two distinct models of transverse-only nonlinear string vibration in a single polarization

are presented in Section 2, including the Kirchhoff-Carrier model, and that simplified from the more general pointwise nonlinear model from Morse and Ingard (1968). Loss and forcing terms are included, and energy balances are presented in the case of both models. Semi-discrete forms for both models are presented for both systems in Section 3, using both local spatial difference operations, and exact modal representations. Energy balances follow through to this semi-discrete case. Time discretisation strategies are presented in Section 4—the maintenance of non-negativity for the discrete time energy leads to numerical stability conditions. Numerical results are presented in Section 5, illustrating energy balances and convergence results for both the Kirchhoff-Carrier system and the transverse pointwise nonlinear system. Some concluding remarks follow in Section 6.

2. MODELS OF NONLINEAR STRING VIBRATION

A general nonlinear model for the transverse vibration of a stiff string in a single polarization is of the following form:

$$(\rho A\partial_t^2 - \mathcal{L})u = \mathcal{F} + \delta(x - x_i)f(t), \tag{1}$$

with:

$$\mathcal{L} = T_0\partial_x^2 - EI\partial_x^4 - 2\rho A(\sigma_0 - \sigma_1\partial_x^2)\partial_t, \tag{2}$$

Here, $u = u(x,t) : [0,L] \times \mathbb{R}_0^+ \to \mathbb{R}$ represents the transverse displacement of a string of length L as a function of a spatial coordinate x and time t; ∂_x^j and ∂_t^j represent the j-th partial derivative with respect of x and t respectively, and $\mathcal{F} = \mathcal{F}(q)$ is a generic force density corresponding to a conservative nonlinear contribution, and depends on $q \triangleq \partial_x u$; it takes on various forms, depending on the type of model, that will be specified shortly. ρ is the string's material density in kg $\cdot$ m^{-3}, A is the string's cross-sectional area, and T_0 is the tension in N. The model includes a stiffness term, derived from the Euler-Bernoulli beam theory, written in terms of the Young's modulus E and the moment of inertia I. See Ducceschi and Bilbao (2016). σ_0, $\sigma_1 \geq 0$, are dimensionless numbers regulating, respectively, the frequency-independent and dependent parts of damping (Bilbao (2009)). This form leads to a quadratic loss profile in the frequency domain. More refined loss models, such as the one from Valette and Cuesta (1993), are not considered here for simplicity. $f(t)$ is an external forcing term, and $\delta(x-x_i)$ represents a Dirac delta function, centered at an excitation location $x = x_i$, indicating point-wise forcing. The string is assumed simply supported at both ends, and thus:

$$u(0,t) = \partial_x^2 u(0,t) = u(L,t) = \partial_x^2 u(L,t) = 0. \tag{3}$$

Models such as (1) extend easily to include coupled motion in a second polarization. See, e.g., Morse and Ingard (1968) in the case of a full model, and Rubin and Gottlieb (1996) and Anand (1969) for the simplified case of the Kirchhoff-Carrier model.

2.1 Energy Analysis

Given two real-valued, square-integrable functions $f(x,t)$, $g(x,t)$, defined over the interval $[0,L]$, the spatial inner product and associated norm may be defined as:

$$\langle f, g\rangle = \int_0^L fg\,\mathrm{d}x, \quad \|f\| = \sqrt{\langle f, f\rangle}. \tag{4}$$

An energy balance for equation (1) is obtained by taking the L^2 inner product with $\partial_t u$ over the domain $[0,L]$:

$$\rho A\langle\partial_t u, \partial_t^2 u\rangle - T_0\langle\partial_t u, \partial_x^2 u\rangle + EI\langle\partial_t u, \partial_x^4 u\rangle - \langle\partial_t u, \mathcal{F}\rangle = -2\rho A(\sigma_0\langle\partial_t u, \partial_t u\rangle - \sigma_1\langle\partial_t u, \partial_t\partial_x^2 u\rangle) + \langle\partial_t u, \delta(x-x_i)\rangle f(t).$$

Using integration by parts and boundary conditions (3), leads directly to

$$\dot{\mathrm{H}} = -2\rho A(\sigma_0\|\partial_t u\|^2 + \sigma_1\|\partial_t\partial_x u\|^2) + \partial_t u(x_i)f(t). \tag{5}$$

Here, the total energy takes the form:

$$\mathrm{H} = \frac{\rho A}{2}\|\partial_t u\|^2 + \frac{T_0}{2}\|\partial_x u\|^2 + \frac{EI}{2}\|\partial_x^2 u\|^2 + \mathrm{V}, \tag{6}$$

where V is a nonlinear potential derived from $\mathcal{F}$. When the source term is not present, the energy is exactly conserved.

2.2 Model Types

The simplest possible choice for $\mathcal{F}$ is that of Kirchhoff and Carrier (Carrier (1945)), where the nonlinearity is averaged over the string length:

$$\mathcal{F}_{\mathrm{K}} = \partial_x\left(\frac{EA}{2L}\|q\|^2 q\right), \tag{7}$$

This expression results from various simplifications and reproduces the perceptual feature of amplitude-dependent pitch, or more generally, time variation in pitch or pitch glides when a loss mechanism is present. See, e.g., Bilbao (2009).

A more refined model may be obtained by taking a Taylor series expansion of the potential derived from the geometrically exact theory of beams, following Morse and Ingard (1968), which includes both longitudinal and transverse displacement. For the sake of simplicity in this short contribution, one may also neglect longitudinal motion, as in Bilbao (2005), leading to the following form of the force density:

$$\mathcal{F}_{\mathrm{T}} = \partial_x\left(\frac{EA - T_0}{2}q^3\right). \tag{8}$$

in view of the upcoming use of the SAV numerical algorithm (Shen et al. (2018)), it is useful to express the nonlinear potentials relative to the forces $\mathcal{F}_{\mathrm{K}}$ and $\mathcal{F}_{\mathrm{T}}$, which are found in the energy expression (6):

$$\mathrm{V}_{\mathrm{K}} = \frac{EA}{8L}\|q\|^4 + \frac{\alpha_0}{2}, \tag{9a}$$

$$\mathrm{V}_{\mathrm{T}} = \frac{EA - T_0}{8}\|q^2\|^2 + \frac{\alpha_0}{2}. \tag{9b}$$

Here, $\alpha_0 > 0$ is an added arbitrary constant shifting the minimum of the potential, but not affecting the motion. Notice that V_{T} is non-negative only if $EA \geq T_0$, which is always true for musical strings. Therefore, both expressions for the nonlinear potential energy are positive semi-definite. The two systems above will be denoted, respectively, K and T for the remainder of the paper.

3. SEMI-DISCRETISATION

In this section, system (1) will be semi-discretised in space, yielding a system of coupled ordinary differential equations (ODEs) in time. To that end, it is first useful to introduce spatial difference operators. The spatial domain is divided into N subintervals of length $h = L/N$, the grid spacing. Doing this yields $N+1$ discretisation points. The

continuous function $u(x,t)$ is then approximated by a grid function $u_l(t) \approx u(lh,t)$, for integer l, $l = 1,\ldots,N-1$ (values of the grid function at the endpoints $l = 0$ and $l = N$ are permanently fixed to zero by the boundary conditions). $u_l(t)$ may be consolidated into an $(N-1)\times 1$ vector $\mathbf{u}(t)$. A simple approximation $\mathbf{D}^-$ to a spatial derivative may be defined as:

$$\mathbf{D}^-\mathbf{u} = h^{-1}([\mathbf{u}^\intercal, 0] - [0, \mathbf{u}^\intercal])^\intercal. \tag{10}$$

Here, $\mathbf{D}^-$ is rectangular, of dimension $N \times (N-1)$. A forward-difference operator is defined as $\mathbf{D}^+ = -(\mathbf{D}^-)^\intercal$, while approximations to second, and fourth order derivatives are $(N-1)\times(N-1)$ matrices, obtained by composition as: $\mathbf{D}^2 = \mathbf{D}^+\mathbf{D}^-$; $\mathbf{D}^4 = \mathbf{D}^2\mathbf{D}^2$. An approximation to q, of size N points, may be defined as: $\mathbf{q} = \mathbf{D}^-\mathbf{u}$ (Bilbao (2005)). Finally, a discretised version of the Dirac delta function at the excitation point $l_0 = \text{floor}(x_i/h)$, is obtained with the column vector $\mathbf{j}$, of length $N-1$, defined as:

$$\mathbf{j}_{l_0} = h^{-1}, \quad \text{otherwise } 0; \tag{11}$$

3.1 Semi-Discrete String Formulation

From the definitions above, it is direct to arrive at a semi-discrete approximation to (1). In view of the application of the SAV numerical algorithm, it is useful to express it in terms of the potentials (9), instead of force densities. Therefore:

$$\rho A\ddot{\mathbf{u}} - \mathfrak{l}\mathbf{u} = h^{-1}\mathbf{D}^+\nabla_{\mathbf{q}}\mathfrak{v} + \mathbf{j}f, \tag{12}$$

where the approximation of the linear operator $\mathcal{L}$ reads:

$$\mathfrak{l} = T_0\mathbf{D}^2 - EI\mathbf{D}^4 - 2\rho A(\sigma_0 - \sigma_1\mathbf{D}^2)\mathrm{d}/\mathrm{d}t, \tag{13}$$

and $\mathfrak{v}$ is a suitable discretisation of the nonlinear potentials $\mathrm{V_K}$, $\mathrm{V_T}$. In particular, semi-discrete forms of (9) are:

$$\mathfrak{v}_\mathrm{K} = \frac{EAh^2}{8L}(\mathbf{q}^\intercal\mathbf{q})^2 + \frac{\alpha_0}{2} \tag{14a}$$

$$\mathfrak{v}_\mathrm{T} = \frac{(EA - T_0)h}{8}(\mathbf{q}^2)^\intercal\mathbf{q}^2 + \frac{\alpha_0}{2}, \tag{14b}$$

where, in the latter equation, the power operator indicates element-wise raising.

3.2 Energy Analysis

Owing to the chain rule, and to the definitions of the difference operators, one has:

$$\dot{\mathfrak{v}} = (\nabla_{\mathbf{q}}\mathfrak{v})^\intercal\dot{\mathbf{q}} = (-\mathbf{D}^+\nabla_{\mathbf{q}}\mathfrak{v})^\intercal\dot{\mathbf{u}}. \tag{15}$$

Then, a discrete energy balance is obtained multiplying equation (12), by $h\dot{\mathbf{u}}^\intercal$. Through summation by parts, one gets:

$$\dot{\mathfrak{h}} = -2\rho Ah\,\dot{\mathbf{u}}^\intercal(\sigma_0 - \sigma_1\mathbf{D}^2)\dot{\mathbf{u}} + h\dot{\mathbf{u}}^\intercal\mathbf{j}f(t), \tag{16}$$

with

$$\mathfrak{h} = \frac{\rho Ah}{2}\dot{\mathbf{u}}^\intercal\dot{\mathbf{u}} - \frac{T_0h}{2}\mathbf{u}^\intercal\mathbf{D}^2\mathbf{u} + \frac{EIh}{2}\mathbf{u}^\intercal\mathbf{D}^4\mathbf{u} + \mathfrak{v}. \tag{17}$$

Thus, the semi-discrete system preserves an energy balance and, given equations (14), the energy is non negative.

3.3 Quadratisation

A fundamental step of the SAV algorithm consists in the quadratisation of the nonlinear potential $\mathfrak{v}$ in the energy expression, through the transformation: $\Psi \triangleq \sqrt{2\mathfrak{v}}$, which is well defined, given the non-negativity of both $\mathfrak{v}_\mathrm{K}$ and $\mathfrak{v}_\mathrm{T}$. After quadratisation, equation (12) can be expressed in terms of Ψ:

$$\rho A\ddot{\mathbf{u}} - \mathfrak{l}\mathbf{u} = -h^{-1}\Psi\mathbf{g} + \mathbf{j}f; \quad \mathbf{g} \triangleq \nabla_{\mathbf{u}}\Psi; \tag{18}$$

where the following relation has been employed:

$$\mathbf{D}^+\nabla_{\mathbf{q}}\mathfrak{v} = -\nabla_{\mathbf{u}}\mathfrak{v} = -\Psi\nabla_{\mathbf{u}}\Psi. \tag{19}$$

The energy balance is unchanged from equation (16), while the expression for conserved energy becomes:

$$\mathfrak{h} = \frac{\rho Ah}{2}\dot{\mathbf{u}}^\intercal\dot{\mathbf{u}} - \frac{T_0h}{2}\mathbf{u}^\intercal\mathbf{D}^2\mathbf{u} + \frac{EIh}{2}\mathbf{u}^\intercal\mathbf{D}^4\mathbf{u} + \frac{\Psi^2}{2}, \tag{20}$$

and, is clearly non-negative.

3.4 Modal Form for the K system

As an alternative approach, system K may be semi-discretised by means of a modal expansion. To that end, the continuous solution u is rewritten as a superposition of time-dependent modal displacements:

$$u(x,t) = \sum_{m=1}^{M} w_m(x)r_m(t). \tag{21}$$

Here M is the number of modes, theoretically infinite, but truncated to a finite integer according to Nyquist requirements. Therefore, equation (21) can be rewritten in vector form: $u(x,t) = \mathbf{w}^\intercal(x)\mathbf{r}(t)$. The corresponding mode shapes $\mathbf{w}$ are found by solving the associated eigenvalue problem of the stiff string under simply supported boundary conditions, as seen in e.g. Bilbao (2004). Thus: $w_m(x) = \sqrt{2/L}\cdot\sin(m\pi x/L)$. Substituting equation (21) into (1), with the force expression given by (7), left-multiplying by $\mathbf{w}$ and taking an L^2 inner product over the string length yields:

$$\ddot{\mathbf{r}} + \mathbf{Q}\dot{\mathbf{r}} + \mathbf{\Omega}^2\mathbf{r} = -\frac{EA}{2L\rho A}(\mathbf{r}^\intercal\mathbf{S}\mathbf{r})\mathbf{S}\mathbf{r} + \frac{1}{\rho A}\mathbf{w}(x_i)f(t), \tag{22}$$

which is the equation describing the time evolution of the modal system. Here, $\mathbf{S}$, $\mathbf{\Omega}$ and $\mathbf{Q}$ are $M\times M$ diagonal matrices, defined as:

$$[\mathbf{S}]_{m,m} = (m\pi/L)^2,$$
$$[\mathbf{\Omega}]_{m,m} = (m\pi/L)\sqrt{T_0/\rho A + (m\pi/L)^2 EI/\rho A},$$
$$[\mathbf{Q}]_{m,m} = 2(\sigma_0 + (m\pi/L)^2\sigma_1).$$

An energy balance is obtained by multiplying equation (22) by $\rho A\dot{\mathbf{r}}^\intercal$:

$$\dot{\tilde{\mathfrak{h}}} = -\rho A\,\dot{\mathbf{r}}^\intercal\mathbf{Q}\dot{\mathbf{r}} + \dot{\mathbf{r}}^\intercal\mathbf{w}(x_i)f(t). \tag{23}$$

Where:

$$\tilde{\mathfrak{h}} = \frac{\rho A}{2}\dot{\mathbf{r}}^\intercal\dot{\mathbf{r}} + \frac{T_0}{2}\mathbf{r}^\intercal\mathbf{S}\mathbf{r} + \frac{EI}{2}\mathbf{r}^\intercal\mathbf{S}^2\mathbf{r} + \underbrace{\frac{EA}{8L}(\mathbf{r}^\intercal\mathbf{S}\mathbf{r})^2}_{\tilde{\mathfrak{v}}}. \tag{24}$$

A quadratised form of system (22) may be obtained by considering the nonlinear potential $\tilde{\mathfrak{v}}$ in equation (24), and writing $\frac{EA}{2L\rho A}(\mathbf{r}^\intercal\mathbf{S}\mathbf{r})\mathbf{S}\mathbf{r} = \nabla_{\mathbf{r}}\tilde{\mathfrak{v}}$. By defining $\tilde{\Psi} \triangleq \sqrt{2\tilde{\mathfrak{v}} + \alpha_0}$ and substituting into equation (22), one obtains the system in quadratised form:

$$\ddot{\mathbf{r}} + \mathbf{Q}\dot{\mathbf{r}} + \mathbf{\Omega}^2\mathbf{r} = -\tilde{\Psi}\tilde{\mathbf{g}} + (\rho A)^{-1}\mathbf{w}(x_i)f(t); \;\; \tilde{\mathbf{g}} \triangleq \nabla_{\mathbf{r}}\tilde{\Psi}. \tag{25}$$

Note that here, the shift constant α_0 has been included directly into the expression for $\tilde{\Psi}$ for brevity. Equation (25) has a form analogous to system (18), and can be solved through the same time-stepping method.

4. TIME DISCRETISATION

Equations (18) and (25) represent two systems of coupled ordinary differential equations, which will now be integrated in time. To this end, time is discretised with a time step k, yielding a sample rate $f_s = 1/k$. Then, a continuous function $u(t)$ is approximated at time step $t = nk$ by the time series u^n, where $n \in \mathbb{N}$ is the time index. The time difference operators are then introduced, as:

$$\delta_{\pm} u^n = \pm(u^{n\pm1} - u^n)/k, \ \delta. u^n = (u^{n+1} - u^{n-1})/2k. \quad (26)$$

The second-difference operator is obtained by combining the operators above:

$$\delta_2 = \delta_+ \delta_- \ . \quad (27)$$

Finally, averaging operators can be written as:

$$\mu_{\pm} u^n = (u^{n\pm1} + u^n)/2, \ \mu. u^n = (u^{n+1} + u^{n-1})/2. \quad (28)$$

The same formal definitions apply to series defined on interleaved time grids, for example: $\delta_+ \Psi^{n-1/2} = (\Psi^{n+1/2} - \Psi^{n-1/2})/k$, where $\Psi^{n+1/2}$ is an approximation to the continuous function $\Psi(t)$ at times $t = (n+1/2)k$. Interleaved grids are commonly found in the literature, see e.g. Yee (1966).

4.1 Numerical Solver

Following Bilbao et al. (2023), a possible discretisation of system (18), based on the SAV method is:

$$\begin{cases} (\rho A \delta_2 - \lambda)\, \mathbf{u}^n = -h^{-1} \mu_+ \Psi^{n-1/2} \mathbf{g}^n + \mathbf{j} f^n \\ \delta_+ \Psi^{n-1/2} = (\mathbf{g}^n)^\intercal \delta. \mathbf{u}^n. \end{cases} \quad (29)$$

Here, $\Psi^{n-1/2}$ is treated as an independent time series that is updated at each time-step. This defines a three-step scheme, where $\mathbf{g}^n$ can be computed analytically as:

$$\mathbf{g}^n = \nabla_{\mathbf{u}} \mathfrak{v}^n / \sqrt{2\mathfrak{v}^n}, \quad (30)$$

and division by zero can be avoided by shifting the potential minimum through the constant α_0 in equation (14). λ is a suitable time discretisation of the linear operator $\mathfrak{l}$, which can take different forms. Here, it was chosen:

$$\lambda = T_0 \mathbf{D}^2 - EI\mathbf{D}^4 - 2\rho A(\sigma_0 \mathbf{I} \delta. - \sigma_1 \mathbf{D}^2 \delta_-). \quad (31)$$

Note the use of the first-order difference operator δ_-. This choice is justified as it allows building the system update matrix in the form of a diagonal matrix plus a rank-1 perturbation, as will be shown shortly. This form is useful when applying the fast inversion formula given later. Second-order-accurate approximations in time are also available, for instance, by applying a centred time difference $\delta.$ to the frequency-dependent damping term. Nevertheless, form (31) ensures a good balance between the accuracy and the efficiency of the numerical scheme since damping terms and usually small. An energy balance for (29) is obtained by multiplying on the left by $h(\delta. \mathbf{u}^n)^\intercal$. Then, following the identities in Bilbao (2009), one gets:

$$\delta_+ \mathfrak{h}^{n-\frac{1}{2}} + E^n = h(\delta. \mathbf{u}^n)^\intercal \mathbf{j} f^n,$$

with

$$E^n = 2\rho A h (\delta. \mathbf{u}^n)^\intercal (\sigma_0 \mathbf{I} - \sigma_1 \mathbf{D}^2) \delta. \mathbf{u}^n; \quad (32)$$

and the energy takes the form

$$\mathfrak{h}^{n-\frac{1}{2}} = \frac{\rho A h}{2} (\delta_- \mathbf{u}^n)^\intercal \left(\mathbf{I} - k\sigma_1 \mathbf{D}^2\right) \delta_- \mathbf{u}^n - \frac{T_0 h}{2} (\mathbf{u}^n)^\intercal \mathbf{D}^2 \mathbf{u}^{n-1} + \frac{EIh}{2} (\mathbf{u}^n)^\intercal \mathbf{D}^4 \mathbf{u}^{n-1} + \frac{(\Psi^{n-\frac{1}{2}})^2}{2}, \quad (33)$$

where $\mathbf{I}$ is the identity matrix. As opposed to the semi-discrete energy (20), expression (33) is not immediately positive semi-definite. Nevertheless, because the nonlinear potential is non-negative, a stability condition for scheme (29) may be obtained by inspecting the linear part alone. Therefore, a sufficient condition for stability is:

$$h \geq \sqrt{\left(\beta + \sqrt{\beta^2 + 16(EI/\rho A)^2 k^2}\right)/2}, \quad (34)$$

where $\beta = 4\sigma_1 k + EIT_0/(\rho A)^2$.

4.2 Update Form

To obtain the update equation for scheme (29), one expands the operators, and substitutes the second equation into the first one; thus:

$$\mathbf{A}^n \mathbf{u}^{n+1} = \mathbf{B}\mathbf{u}^n + \mathbf{C}^n \mathbf{u}^{n-1} - k^2 h^{-1} \mathbf{g}^n \Psi^{n-1/2} + \mathbf{j} f^n. \quad (35)$$

The matrices take the form:

$$\begin{aligned} \mathbf{A}^n &= \rho A(1 + \sigma_0 k)\mathbf{I} + \boldsymbol{\zeta}^n (\boldsymbol{\zeta}^n)^\intercal \\ \mathbf{B} &= 2\rho A \mathbf{I} + (T_0 k^2 + 2\rho A \sigma_1 k)\mathbf{D}^2 - EIk^2 \mathbf{D}^4 \\ \mathbf{C}^n &= \rho A(1 - \sigma_0 k)\mathbf{I} - 2\rho A \sigma_1 k \mathbf{D}^2 + \boldsymbol{\zeta}^n (\boldsymbol{\zeta}^n)^\intercal, \end{aligned} \quad (36)$$

where $\boldsymbol{\zeta}^n = (k/2\sqrt{h})\mathbf{g}^n$. As mentioned above, the update matrix $\mathbf{A}^n$ has the form of a diagonal matrix plus a rank-1 perturbation and admits a fast inversion through the Sherman-Morrison formula (Sherman and Morrison (1950)). $\Psi^{n+1/2}$ is then computed via the second equation in (29), once (35) is solved for $\mathbf{u}^{n+1}$.

4.3 Modal Scheme

The SAV method can be applied to the modal system (25). Therefore, a discrete version reads:

$$\begin{cases} (\delta_2 - \tilde{\lambda})\mathbf{r}^n = -\mu_+ \tilde{\Psi}^{n-1/2} \tilde{\mathbf{g}}^n + (\rho A)^{-1} \mathbf{w}(x_i) f^n \\ \delta_+ \tilde{\Psi}^{n-1/2} = (\tilde{\mathbf{g}}^n)^\intercal \delta. \mathbf{r}^n, \end{cases} \quad (37)$$

with:

$$\tilde{\lambda} = -\boldsymbol{\Omega}^2 - \mathbf{Q}\delta. \ . \quad (38)$$

$\tilde{\mathbf{g}}^n$ can be computed analytically, as seen in equation (30): $\tilde{\mathbf{g}}^n = \nabla_{\mathbf{r}} \tilde{\mathfrak{v}}^n / \sqrt{2\tilde{\mathfrak{v}}^n}$, and division by zero can be avoided by shifting the potential through the constant α_0. An energy analysis, not shown here for brevity, is run by multiplying the first equation in (37) by $\rho A(\delta. \mathbf{r}^n)^\intercal$, and yields a stability condition that links the sampling step k to the highest eigenfrequency inside $\boldsymbol{\Omega}$: $k \leq 2/\omega_M$. This condition can be employed to retrieve a limit for the number of modes M, related to the sampling frequency. Scheme (37) can be expanded to obtain an update equation entirely equivalent to (35).

5. NUMERICAL TESTING

5.1 System K

Figure 1 displays the time solution, the energy error and the spectrogram of system (29), with potential (14a). Here, the energy error is defined as:

$$\Delta H^{n+1/2} = 1 - (H_{\text{tot}}^{n+1/2})/(\mathfrak{h}^{1/2}) \quad (39)$$

where $H_{\text{tot}}^{n+1/2} = \mathfrak{h}^{n-1/2} + \sum_{\nu=0}^{n} E^\nu k$. From the second plot it is observed that the energy is indeed conserved, with an

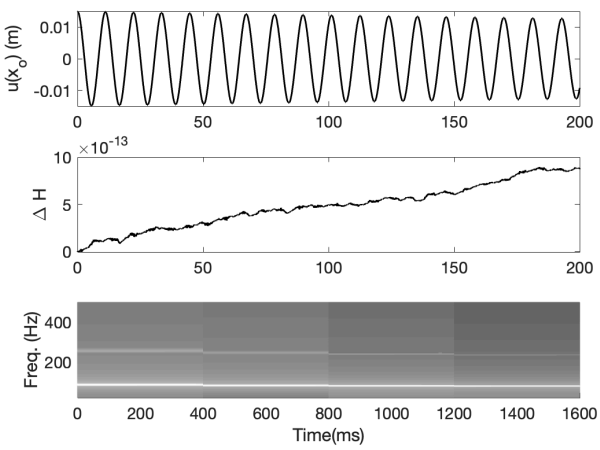

Fig. 1. Waveform, energy error and spectrogram of system (29) with potential K. Physical parameters are: $\rho = 8 \times 10^3$ Kg/m^3, $T_0 = 75$ N, $A = 3.97 \times 10^{-7}$ m^2, $E = 174$ GPa, $I = 1.25 \times 10^{\times}10^{-14}$ m^4, $\sigma_0 = 0.92$, $\sigma_1 = 2.86 \times 10^{-4}$. The output point x_o is exactly at half string. The system is initialised in its first mode of vibration, with an amplitude of 1.5 cm, and run at OF = 10.

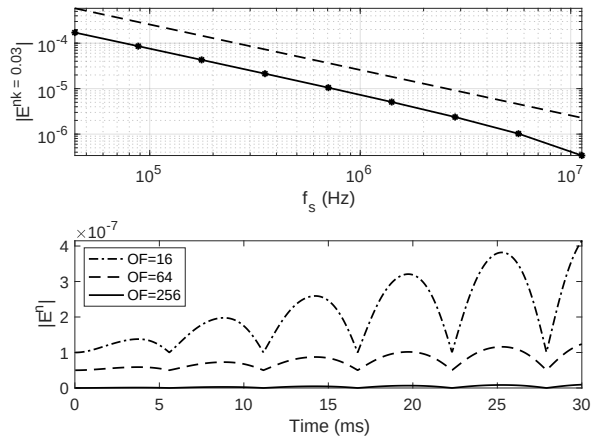

Fig. 2. Convergence test for system K. The target solution is obtained at OF = 512. The SAV scheme is run at OF = 2^a, with $a = [0, 8]$ integer. String parameters and initialisation are as listed in Figure 1. The dashed plot in the first panel represents a line with a slope of -1, for comparison.

error within the order of machine accuracy. Note that the upward drift is entirely related to round-off effects due to finite precision, not discussed in this paper. The different time zooming on the third panel allows to show the pitch glide provided by the nonlinear term; nonlinear behaviour is also highlighted by the presence of a second peak in the spectrum.

A convergence test is now performed. A "target" solution is computed with an energy-conserving, model-specific integrator from Bilbao (2009), run at a high oversampling factor (OF). Its form is not reported here for brevity. Here, OF is an integer factor such that the final sample rate is OF $\times$ 44.1 kHz (44.1 kHz is a standard audio sample rate). Then, an error is computed, between the target solution and solutions computed with system (29), run with an

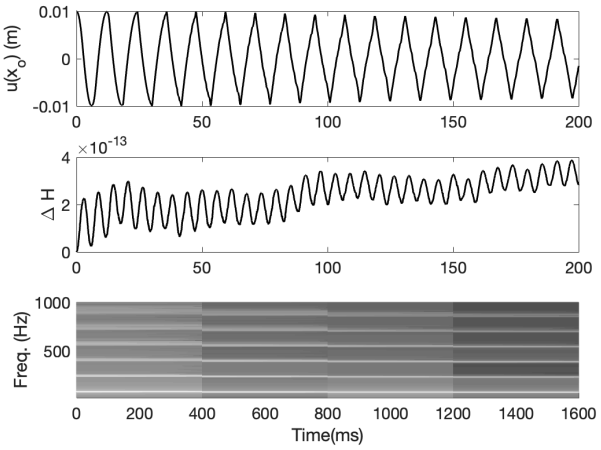

Fig. 3. Waveform, energy error and spectrogram of system (29) with potential T. String parameters are as listed in Figure 1. The system is initialised in its first mode of vibration, with an amplitude of 1 cm, and run at OF = 10.

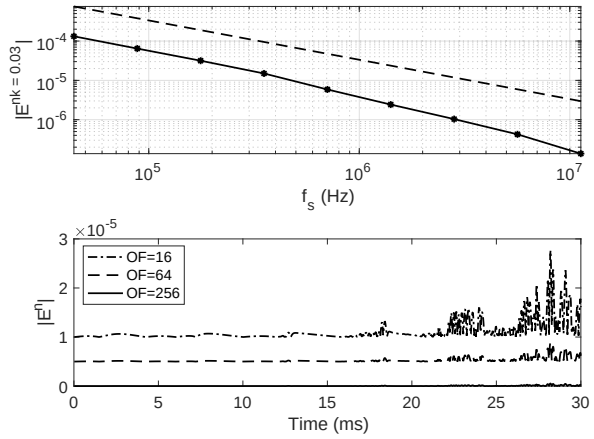

Fig. 4. Convergence test for system T. The target solution and the SAV scheme are run at the same OFs listed in Figure 2. String parameters are as listed in Figure 1. The string is initialised in its first mode of vibration, with an amplitude of 1 cm

increasing OF. Results are displayed in Figure 2. The first panel represents the error of scheme (29), at time $nk = 0.03$ s, computed at an increasing OF and plot in logarithmic scale along with a line of slope -1. The error is defined as $E^n = \hat{u}^n - u^n$, where $\hat{u}$ is the target solution. The second panel shows the evolution of the error over time for three solutions, computed at different sample rates. An increasing offset of 5×10^{-8} is added to the plots to improve readability. A comparison with the line of slope -1 indicates that the error decreases with an order k, making the scheme first-order accurate. This is expected, given the explicit discretisation of the frequency-dependent damping term, and the fourth-order spatial operator, that lead to the stability condition (34). Similar results were obtained with the modal scheme (37), and are not shown here for brevity.

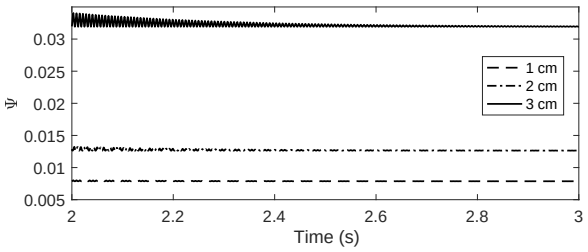

Fig. 5. Evolution of Ψ over time for System T. The string was initialised with increasing amplitudes of $1, 2$ and 3 cm, and the scheme was run at OF $= 10$. The string physical values are as in Figure 1.

5.2 System T

Figure 3 shows the temporal evolution, the energy error and the spectrogram of system (29), with potential (14b). It is possible to see that this potential introduces a stronger nonlinear behaviour, which is now also clearly visible from the time domain plot. Energy is still conserved; however, the error presents more oscillations than in the previous case.

The same convergence test employed for system K was run in this case. As before, the target solution is computed with an energy conserving, model-specific method proposed by Bilbao (2005), run at a high OF. Results are displayed in Figure 4; in the second panel, an increasing offset of 5×10^{-6} is added to the plots to improve readability. The time evolution of the error now presents higher oscillations than for system K. However, first order-accuracy still emerges from the first panel, indicating numerical convergence of the SAV algorithm.

During testing of system T, an anomalous behaviour of the auxiliary variable $\Psi^{n-1/2}$ was observed, which is reported in Figure 5. Here, system T is initialised with different amplitudes, and the same potential shift $\alpha_0 = 3{\times}10^{-5}$. For higher initial displacements, Ψ does not decay at its theoretical minimum, $\sqrt{\alpha_0}$. This behaviour was not observed in system K; furthermore, for higher OFs, the Ψ minimum converges at the theoretical minimum. Nevertheless, this anomalous effect requires further investigation.

6. CONCLUSION

Two discrete models depicting nonlinear transverse vibrations in strings were introduced: the Kirchhoff-Carrier model and a simplified transverse-only version derived from Morse and Ingard's pointwise model. Spatial discretization of the equations was achieved through the use of finite difference operators, and exact modal representations in the case of the Kirchhoff-Carrier model. The Scalar Auxiliary Variable (SAV) method was subsequently employed, initially by approximating the nonlinear energies through a scalar auxiliary state variable, followed by temporal integration of the resulting systems using a commonly used explicit time-stepping procedure. Comparative analysis was conducted with respect to benchmark integration techniques found in the existing literature. The experimental findings demonstrated that the SAV algorithm converges towards the model-specific methods when the sampling rate is sufficiently high. Notably, in the case of the simplified Morse-Ingard model, an anomalous behaviour of the auxiliary variable was observed, which is mitigated at higher sampling rates. However, it warrants further investigation.

ACKNOWLEDGEMENTS

This work was supported by the European Research Council (ERC), under grant 2020-StG-950084-NEMUS.

REFERENCES

Anand, G. (1969). Large-amplitude damped free vibration of a stretched string. *J. Acoust. Soc. Am.*, 45(5), 1089–1096.

Bank, B. and Sujbert, L. (2005). Generation of longitudinal vibrations in piano strings: From physics to sound synthesis. *J. Acoust. Soc. Am.*, 117, 2268–2278.

Bilbao, S. (2009). *Numerical Sound Synthesis*. John Wiley & Sons, Ltd, Chichester, UK.

Bilbao, S. and Smith III, J.O. (2005). Energy-conserving finite difference schemes for nonlinear strings. *Acta Acust. united Acoust.*, 91(2), 299–311.

Bilbao, S. (2004). Modal-Type Synthesis Techniques for Nonlinear Strings with an Energy Conservation Property . In *Proc. Digital Audio Effects (DAFx-04)*, 119–124. Naples, Italy.

Bilbao, S. (2005). Conservative numerical methods for nonlinear strings. *J. Acoust. Soc. Am.*, 118(5), 3316–3327.

Bilbao, S., Ducceschi, M., and Zama, F. (2023). Explicit exactly energy-conserving methods for hamiltonian systems. *J. Comput. Phys.*, 472, 111697.

Carrier, G.F. (1945). On the non-linear vibration problem of the elastic string. *Q. Appl. Math.*, 3(2), 157–165.

Chabassier, J., Chaigne, A., and Joly, P. (2013). Modeling and simulation of a grand piano. *J. Acoust. Soc. Am.*, 134, 648—-665.

Dickey, R. (1969). Infinite systems of nonlinear oscillation equations related to the string. *Proc. Amer. Math. Soc.*, 23(3), 459–468.

Dickey, R. (1980). Stability of periodic solutions of the nonlinear string. *Q. App. Math.*, 38, 253–259.

Ducceschi, M. and Bilbao, S. (2016). Linear stiff string vibrations in musical acoustics: Assessment and comparison of models. *J. Acoust. Soc. Am.*, 140(4), 2445–2454.

Ducceschi, M. and Bilbao, S. (2022). Simulation of the geometrically exact nonlinear string via energy quadratisation. *J. Sound Vib.*, 534(4), 117021.

Gough, C. (1984). The nonlinear free vibration of a damped elastic string. *J. Acoust. Soc. Am.*, 75(6), 1770–1776.

Kirchhoff, G. (1883). *Vorlesungen über Mechanik*. Tauber, Leipzig.

Kurmyshev, E. (2003). Transverse and longitudinal mode coupling in a free vibrating soft string. *Phys. Lett. A*, 310(2–3), 148–160.

Lopes, N., Hélie, T., and Falaize, A. (2015). Explicit second-order accurate method for the passive guaranteed simulation of port-hamiltonian systems. In *Proc. 5th IFAC 2015*. Lyon, France.

Morse, P. and Ingard, U. (1968). *Theoretical Acoustics*. Princeton University Press, Princeton, NJ, USA.

Narasimha, R. (1968). Nonlinear vibration of an elastic string. *J. Sound Vib.*, 8(1), 134–146.

Oplinger, D. (1960). Frequency response of a nonlinear stretched string. *J. Acoust. Soc. Am.*, 32, 1529–1538.

Roze, D. and Hélie, T. (2008). Sound synthesis of a nonlinear string using Volterra series. *J. Sound Vib.*, 314(1–2), 275–306.

Rubin, M. and Gottlieb, O. (1996). Numerical solutions of forced vibration and whirling of a nonlinear string using the theory of a cosserat point. *J. Sound Vib.*, 197(1), 85–101.

Shen, J., Xu, J., and Yang, J. (2018). The scalar auxiliary variable (SAV) approach for gradient flows. *J. Comput. Phys.*, 353, 407–416.

Sherman, J. and Morrison, W.J. (1950). Adjustment of an inverse matrix corresponding to a change in one element of a given matrix. *Ann. Math. Stat.*, 21, 124–127.

Valette, C. and Cuesta, C. (1993). *Mécanique de la corde vibrante*. Hermès, Paris.

Yang, X. and Han, D. (2016). Linearly first- and second-order, unconditionally energy stable schemes for the phase field crystal model. *J. Comput. Phys.*, 330, 1116–1134.

Yang, X., Zhao, J., and Wang, Q. (2017). Numerical approximations for the molecular beam epitaxial growth model based on the invariant energy quadratization method. *J. Comput. Phys.*, 333, 104–127.

Yee, K. (1966). Numerical solution of initial boundary value problems involving maxwell's equations in isotropic media. *IEEE Trans. on Antennas Propag.*, 14(3), 302–307.